JOURNAL OF CATALYSIS 119, 201–214 (1989)

Mechanism of Catalyzed Graphite Oxidation by Monolayer Channeling and Monolayer Edge Recession

PETER J. GOETHEL AND RALPH T. YANG[1]

Department of Chemical Engineering, State University of New York at Buffalo, Buffalo, New York 14260

Received November 18, 1988; revised May 8, 1989

Monolayer channeling (i.e., channeling at one graphite layer depth) on the basal plane of graphite is revealed for catalysts in the graphite–oxygen reaction by employing gold decoration/TEM. Rates and mechanisms of monolayer channeling have been studied for Pt, Cu, V, and V_2O_5. The breakage of carbon–carbon bonds at the Pt and edge graphite interface is the rate-limiting step for Pt-catalyzed oxidation. An oxygen transfer mechanism appears to be operative in the vanadium-catalyzed oxidation, and the rate-limiting step is the oxidation of the surface of the particle which is in the reduced state of V_6O_{13}. The rate-limiting step for the copper-catalyzed reaction is a step occurring at the interface between the catalyst and edge graphite, either by the breakage of carbon–carbon bonds or the oxidation of edge carbon by CuO. Vanadium oxide also undergoes catalyzed monolayer edge recession, forming elongated hexagonal etch pits which are bound by $\langle 11\bar{2}0 \rangle$ (zig-zag) edges. It is shown that there are two different graphite zig-zag steps exhibiting different reactivities which result in the unique shape of the pits. By comparing the monolayer channeling rates with the rates for deep-layer channeling reported in the literature, it is concluded that the relative contribution to the total oxidation rates by monolayer channeling is at least as important as that by deep channeling.

INTRODUCTION

Much attention has been attracted to the behaviors and catalytic actions of catalysts (metals, metal oxides, and salts) in the gas–carbon reactions. The most important gas–carbon reactions involve O_2, CO_2, H_2O, or H_2 as the reactant. Although it has been known for many years that small amounts of catalysts can have dramatic effects on the rates of these reactions (*1, 2*), our present understanding of the catalytic behavior is attained primarily from studies using microscopy. These studies have progressed from optical microscopy (*3*) to various techniques of electron microscopy, e.g., etch-decoration TEM (*4*) and controlled-atmosphere TEM (*5*).

A unique and most intriguing phenomenon associated with the catalyzed gas–graphite reactions is the motion of the catalyst on graphite which results in the catalytic activity. A number of catalyst motions (or actions) have been observed. The most extensively studied catalyst actions are pitting (*1, 6*), deep channeling (part of the extensive work by Baker has been reviewed in Refs. (*7, 8–11*)), and deep edge recession (*12, 13*). The two latter actions refer to the carving of channels and receding of line edges by the catalysts both of which involve many graphite layers, hence the term "deep" channeling. These two actions have been studied by using mainly controlled-atmosphere TEM.

The controlled-atmosphere TEM technique, however, relies on the relative contrast of images which requires channels many graphite layers deep (e.g., >30 layers) and consequently "overlooks" catalytic events occurring on the surface layers of graphite. By using gold decoration, monolayer (single graphite layer) channeling and pitting by catalysts have been revealed and investigated in this laboratory (*14–17*). The mechanistic steps involved in

[1] To whom correspondence should be addressed.

0021-9517/89 $3.00

monolayer channeling in graphite hydrogenation ($C + 2H_2 \rightarrow CH_4$) by Pt, Ni, and Ru are reasonably understood (*15–17*). More important, the relative contribution to the total hydrogenation rates by monolayer channeling is at least as important as that by deep channeling (*17*).

In this paper, first results of monolayer channeling and pitting by catalysts in the graphite–oxygen reaction are presented. Some of the most extensively investigated catalysts for the $C + O_2$ reaction (Cu, Pt, V, and V_2O_5) were selected for this study.

EXPERIMENTAL

The carbon used was a natural, single-crystal graphite from Ticonderoga, New York. This graphite was chosen for its well-defined crystalline structure and ability to be cleaved into specimens thin enough (700 to 1000 Å thickness) for TEM observation while maintaining a large single-crystal basal plane area. A detailed explanation of the techniques used to prepare the crystals for reaction, catalyst deposition, and subsequent gold decoration has been given elsewhere (*15, 18, 19*).

The catalysts were all of puratronic grade (supplied by Alfa Products, Danvers, MA) with the following purities: Cu (99.999%), Pt (99.99%), V (99.97%), and V_2O_5 (99.995%). The hydrogen and helium used for reduction and inert carrier, respectively, were of ultrahigh purity (99.999% minimum purity for both), and were further subjected to a stringent liquid-N_2 trap system (described in Ref. (*15*)) to remove traces of O_2, H_2O, and CO_2. The Pt, Cu, and V were available in the form of wires and were deposited on the cleaved graphite basal plane by vacuum evaporation. Vanadium pentoxide was deposited via an alcohol suspension. The graphite samples containing catalyst were placed on a sapphire plate held in an alumina combustion boat. This boat was placed in a quartz tube furnace. The overnight degassing of the sample was carried out in hydrogen as required to preserve the single-crystal basal plane from reaction with the surface oxides which decompose upon heating. After a 12-h purge in hydrogen at 450°C the gas flow was switched to helium and sufficient time was allowed to assure complete removal of hydrogen (approximately 30 min). The system was then raised to the desired reaction temperature. Control experiments were performed where the samples were left in the helium at the reaction temperature for at least three times the reaction time to be used (e.g., 30 min if a 10-min reaction in O_2 was to be performed). The samples were next decorated with gold nuclei and viewed in TEM. No reaction was observed to take place before introducing the oxygen environment. For the oxygen reaction a 0.1-atm mixture of oxygen in helium was passed over the sample for the desired reaction time. Other experimental details were the same as those described elsewhere (*15, 19*).

For rate calculations, only channels with clearly defined both beginnings and ends were used. However, the majority of channels were not useful for rate calculations due to interferences with other channels and steps on the surface. The rate data were measurable to two significant figures for a given channel. The scatter of the rate data among different channels was generally within 10%, as is the case with rate measurements for deep channeling (*5, 20–22*) and pitting (*3, 4, 6, 18*).

RESULTS AND DISCUSSION

Monolayer channeling has been reported only for the graphite–hydrogen reaction (*15–17*). The first objective of this study was to determine whether monolayer channeling also occurs in the graphite–oxygen reaction. Employing the same techniques used for the graphite–hydrogen reaction (*15*) monolayer channels were observed in the graphite–oxygen reaction by all four catalysts, Pt, Cu, V, and V_2O_5 (*19*). The proof for the monolayer channel and its origin have been discussed elsewhere (*15, 19*). Monolayer channels and pits are initi-

ated from lattice vacancies and monolayer steps. The kinetics and mechanistic steps for monolayer channeling and pitting in graphite oxidation are discussed below.

Rationale for Determining the Rate-Limiting Step in Monolayer Channeling

The deep channeling action by catalysts in the graphite–oxygen reaction has been studied by Baker *et al.* for Pt (*20*), Cu (*21*), V/V_2O_5 (*22*), and other metals/metal oxides. The following sequential steps are generally involved in deep channeling as well as monolayer channeling (*15–17*):

1. breaking of carbon–carbon bonds at the carbon–catalyst interface located at the advancing front of the catalyst;
2. transport of carbon (*15–17*) or oxygen ions/atoms (*23, 24*) through the catalyst particle and
3. oxidation (or hydrogenation) of carbon at the catalyst–gas interface.

For deep channeling in the graphite–oxygen reaction, Baker *et al.* (*20–22*) showed that the speed of channeling is inversely proportional to the catalyst particle size, indicating that diffusion of carbon through the catalyst particle is the rate-limiting step.

Figure 1 illustrates the carbon diffusion paths for deep channeling and for monolayer channeling. In deep channeling the maximum resistance to diffusion arises from carbon atoms at the bottom of the catalyst–carbon interface. These atoms must diffuse at least the difference of the channel depth before reaching a reactive catalyst–gas interface. In monolayer channeling the resistance to diffusion is essentially zero, as the minimum distance for diffusion is only one atomic step. This suggests two possible rate-limiting steps for monolayer channeling in the graphite–oxygen reaction when deep channeling shows diffusion limitation.

The first possibility is that monolayer channeling remains diffusion limited. A numerical calculation of this diffusion/reaction problem shows no particle size dependence on the channel propagation rate (*19, 25*). The reason for this lack of size dependence can also be understood qualitatively by considering the concentration profile of carbon along the catalyst–gas interface, as shown in Fig. 2. The concentration of carbon in the catalyst at the point of contact between catalyst and graphite is assumed as the solubility of carbon in the catalyst at the reaction temperature. The carbon concentration declines very rapidly due to the fast reaction between surface carbon and oxygen. In our model calculation for the Pd–graphite–O_2 system, the concentration of carbon decreased to essentially zero in approximately 50 Å regardless of the particle size. Thus all particles greater than 50 Å would channel at the same speed.

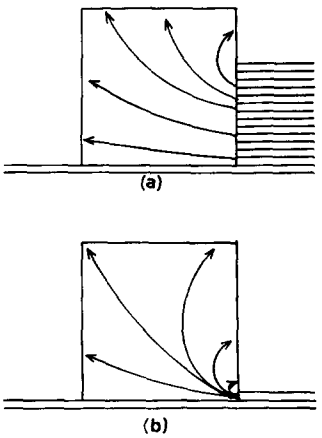

FIG. 1. Schematic of carbon diffusion paths in deep channeling (a) and in monolayer channeling (b). Graphite layers are indicated by parallel lines and the catalyst (represented by a cube) channels to the right.

A second possibility is the breaking of the carbon–carbon bonds becoming the rate-limiting step; the breakage occurs at the graphite monolayer step (where the edge carbon atom has an unpaired sp^2 electron) by the influence of the catalyst. Such a rate-limiting step has been suggested for catalyzed gas–carbon reactions from bulk reaction results (using mixed graphite and catalyst powders) (*23, 26, 27*). In our mod-

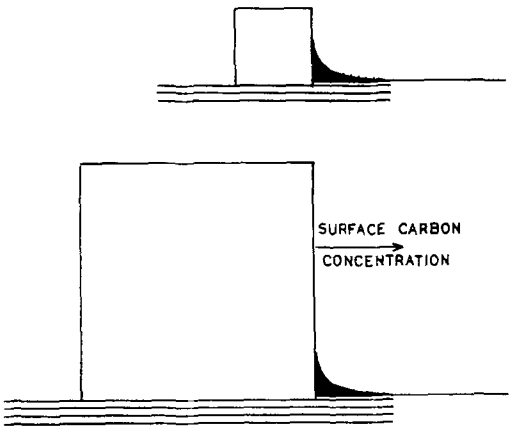

FIG. 2. Carbon concentration profile in catalyst particle away from the graphite step. For the Pd–C–O_2 system the concentration declines to zero at approximately 50 Å from the step. (Two particles both larger than 50 Å are shown. For smaller particles the concentration rises above zero while maintaining a zero slope at the top.)

eling calculations (*19, 25*) it was assumed that the carbon–carbon bond breakage occured much faster than the diffusion step or the surface reaction step. This was a rational assumption for deep channeling in which the carbon–carbon bond breakage would result in the same channeling speed for all particle sizes. In monolayer channeling, however, the diffusion resistance is very small and the possibility of carbon–carbon bond breakage being the rate-limiting step cannot be excluded. A carbon–carbon bond breakage rate-limiting step for monolayer channeling would also result in a lack of dependence of channeling speed on particle size.

It is seen that both rate-limiting possibilities for monolayer channeling would result in all size particles traveling at the same speed. The experimental data showed that this was indeed the case for Pt and Cu catalysts. To distinguish between carbon–carbon bond breakage limitation and carbon diffusion limitation the magnitude of the monolayer channeling propagation speed can be compared with the rate calculated from a diffusion controlled model and the rate of deep channeling. If the rate is greater than that of the fastest deep channeling particle, and significantly less than the diffusion limited case, then carbon–carbon bond breakage is likely the rate-limiting step.

Monolayer Channeling by Pt

Pt–catalyzed graphite oxidation was studied at 750°C and 0.1 atm oxygen. Vacuum evaporation of Pt onto the basal plane of graphite produced dispersed particles with a wide size distribution, from below 40 nm to nearly 1 μm. As demonstrated earlier (*15*), monolayer channeling can be initiated only from lattice vacancies in the basal plane surface or from monolayer steps. Both monolayer channels and monolayer etch pits were seen on the reacted graphite samples, as revealed by the gold nuclei. Figure 3 is a typical TEM picture of the reacted graphite surface. A quantitative analysis of the monolayer channels cut by particles ranging in size from 48 to 512 nm showed the same channeling speed of 24 ± 2 nm/s. This result was different from that of deep channeling for the same reaction system, where the channeling speed was inversely proportional to the Pt size (*20*).

For deep channeling by Pt in the graphite–O_2 reaction at 750°C, Baker *et al.* (*20*) reported a channeling of 3 nm/s for 20-nm particles. Thus, for the same particle size, the monolayer channeling speed was much higher than the deep channeling speed. Assuming carbon diffusion limitation, the speed of monolayer channeling by Pt particles at 750°C was predicted using model calculations (*19, 25*). The predicted value for monolayer channeling speed was 1.0×10^3 nm/s for all particle sizes greater than 20 nm. This was much higher than the observed value. From the discussion in the preceding section, it is seen that the breakage of carbon–carbon bonds is the rate-limiting step for monolayer channeling by Pt.

The channel orientation was determined by comparing the TEM picture and the

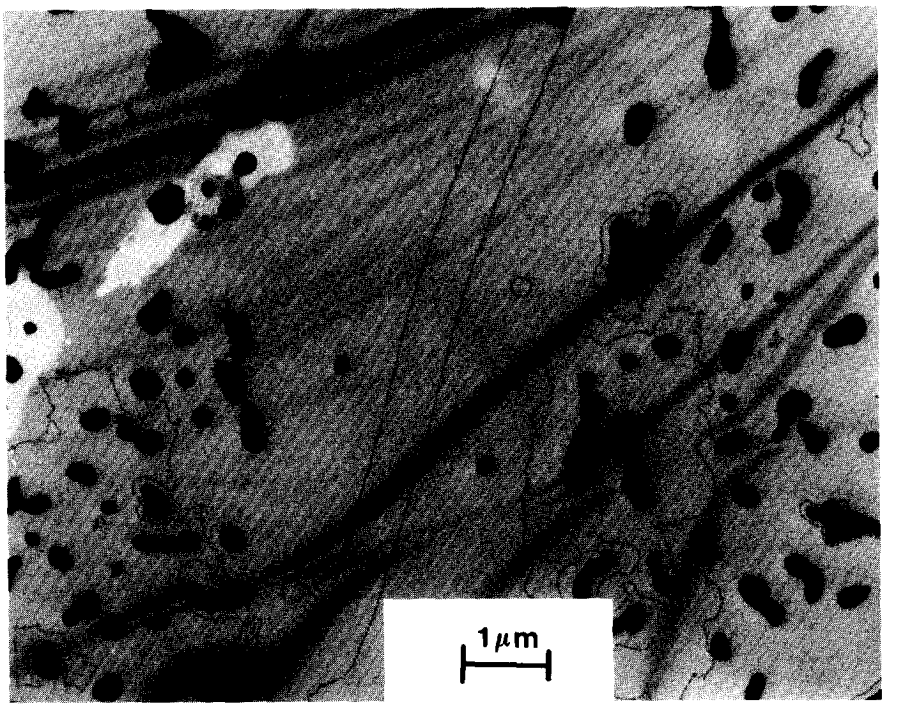

FIG. 3. TEM picture of gold-decorated basal plane of graphite showing a monolayer channel carved by a Pt particle at 750°C in 0.1 atm O_2 for 355 s, also showing monolayer etch pits, by both catalyzed and uncatalyzed oxidation. (Small dots are gold nuclei and irregularly shaped particles are Pt.)

selected area electron diffraction of the substrate graphite. The comparison showed that the two sides of the channel were oriented along the $\langle 11\bar{2}0 \rangle$ (zig-zag) crystal direction.

Large Pt particles produced parallel-sided monolayer channels, as shown in Fig. 3. Figure 4 shows a monolayer channel which was fluted in appearance. Fluted-shaped channels were seen for all particles smaller than approximately 40 nm. Figure 4 also shows etch pits produced from the uncatalyzed oxygen reaction with lattice vacancies. The diameter of the etch pits was approximately equal to the width of the channel where the channel originated. This result is expected as the width of the channel is proportional to the amount of time the channel wall is exposed to the reactive gas for uncatalyzed attack. The pit diameter correlates to a turnover frequency of 3.0 C atoms gasified/C atom site × s, in agreement with the rates of uncatalyzed oxygen etch pit formation (*28*).

Monolayer Channeling by Cu

In the graphite–oxygen reaction, Cu was found to be an active deep channeling catalyst, likely in the form of CuO (*21, 29*). This reaction was included in this study using dispersed copper particles (below 1 μm size) on the basal plane of graphite. The reaction was conducted at 550°C in 0.1 atm O_2. A typical result is given in Fig. 5, which shows a monolayer channel. From a quantitative analysis of the channeling speeds, it was concluded that particles of all sizes formed monolayer channels at the same speed of 45 ± 5 nm/s.

The deep channeling speed for the same reaction system at the same temperature was reported to be 1.6 nm/s for 25 nm particles (*21*). This is, again, much lower than the monolayer channeling speed. The-

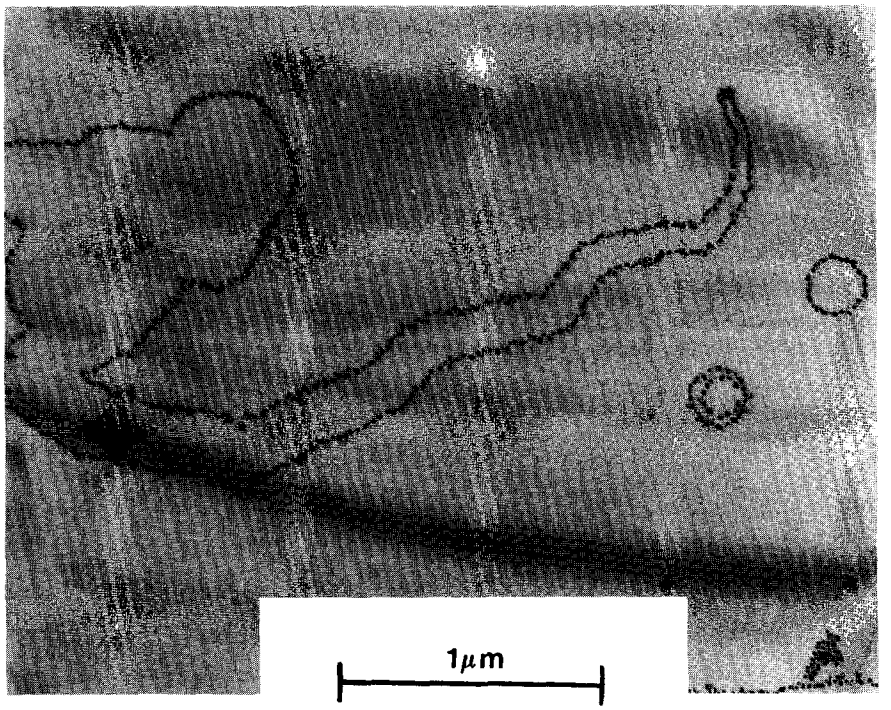

FIG. 4. TEM picture of gold-decorated graphite showing a monolayer channel by Pt at 750°C in 0.1 atm for 355 s (see more details in Fig. 3 caption).

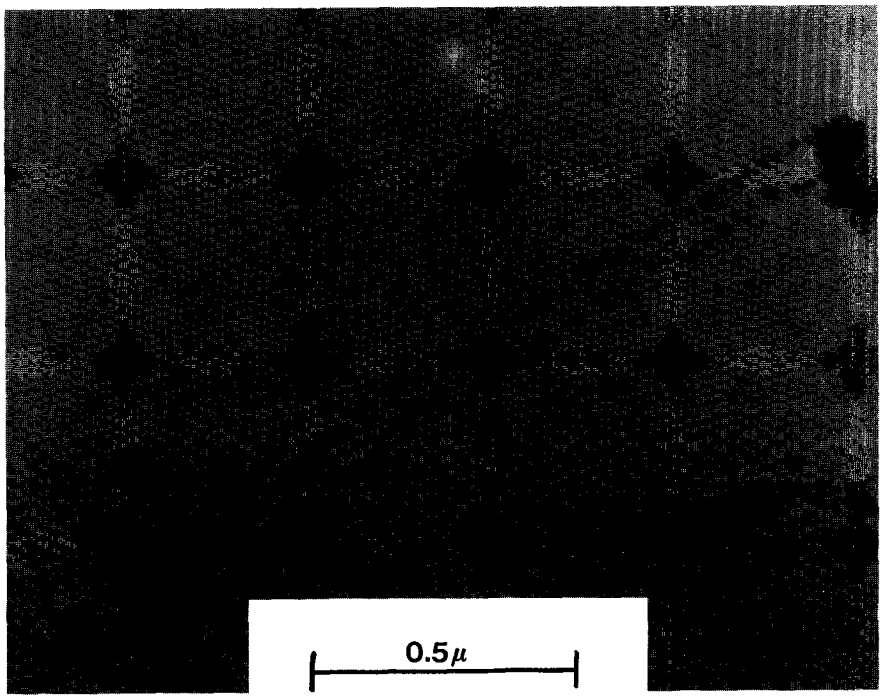

FIG. 5. Monolayer channel carved by Cu at 550°C in 0.1 atm O_2 for 380 s (see more details in Fig. 3 caption).

oretical calculations of the diffusion-limited monolayer channeling speed has not been performed due to a lack of information on the transport of carbon through/on the CuO particle. And, in fact, the mechanism could involve the transfer of oxygen to the catalyst–carbon interface (*29*). However, using a low "diffusivity" value of 10^{-9} cm^2/s, values of the order of hundreds of nm/s would be obtained for the diffusion-limited monolayer channeling (*19, 25*). This comparison once again suggests that the breakage of carbon–carbon bonds is the rate-limiting step in monolayer channeling by copper.

The monolayer channeling rates by copper are higher than that by platinum, indicating a faster carbon–carbon bond breakage by copper. The oxidation state of copper at the carbon–copper interface and the mechanism for carbon–carbon bond breakage is not clear at this point. McKee (*29*) suggested that CuO is reduced to Cu and CO at the CuO–graphite interface. Accordingly, a deficiency of oxygen at this interface would be replenished by either lattice oxygen or surface oxygen (see the discussion by Holstein and Boudart (*23*)) from the gas–catalyst interface. If this is indeed the mechanism for monolayer channeling by CuO, our results would indicate that the reduction of CuO at the CuO–C interface is the rate-limiting step.

Monolayer Channeling by V_2O_5

The catalyzed graphite–oxygen reaction was studied at 600°C in 0.1 atm O_2. Graphite samples separately deposited with V metal and V_2O_5 on the basal plane were used. Identical results were obtained with these two catalysts indicating that the same active species was operative. The predominant modes of catalytic action were channeling and catalyzed etch pit recession; the latter will be discussed in the ensuing section.

Figure 6 illustrates typical monolayer channels formed by large and small particles. In contrast to the results with Pt and Cu catalysts, the V_2O_5 monolayer channels displayed a clear particle size dependence. The monolayer channeling speed was found to be proportional to particle size. This size dependence is contrary to all previously observed dependence for deep channeling in catalyzed graphite–oxygen reaction (see the work by Baker *et al.*). Baker *et al.*, however, did not attempt to measure the size dependence in their study of deep channeling by V_2O_5 (*22*). The size dependence for monolayer channeling by V_2O_5 is plotted in Fig. 7, in terms of total gasification rate per particle against particle surface area exposed to oxygen (by assuming hemispherical shape). The results in Fig. 7 indicate that the rate-limiting step is a reaction occurring on the surface exposed to O_2.

The V_2O_5 catalyzed $C–O_2$ reaction has been studied by McKee (*24*) and Baker *et al.* (*22*). V_6O_{13} was identified by XRD in the mixture of V_2O_5 and carbon after heating in N_2 (*24*). The TGA data were consistent with the XRD finding (*24*). In the controlled-atmosphere TEM study of deep channeling in the presence of oxygen (5 Torr), V_6O_{13} was also revealed by electron diffraction in the TEM (*22*). A reduction–oxidation mechanism for the catalyzed reaction was suggested for McKewe (*24*), which involves reduction to V_6O_{13} at the catalyst–carbon interface and oxidation of V_6O_{13} to V_2O_5 at the O_2–catalyst interface.

Our results and the above discussion suggest a redox or oxygen transfer mechanism for monolayer channeling by V_2O_5. Carbon is gasified to oxides at the carbon–catalyst interface by combining with two O atoms from V_2O_5, forming V_6O_{13}, and the bulk of the catalyst particle remains as V_6O_{13}. Oxygen is replenished from the gas phase on the surface of the particle, and O atoms are transported either through the bulk lattice or on the surface to the carbon–catalyst interface where carbon gasification takes place. Furthermore, the results shown in Fig. 7 suggest that an oxidation reaction on the catalyst surface is the rate-

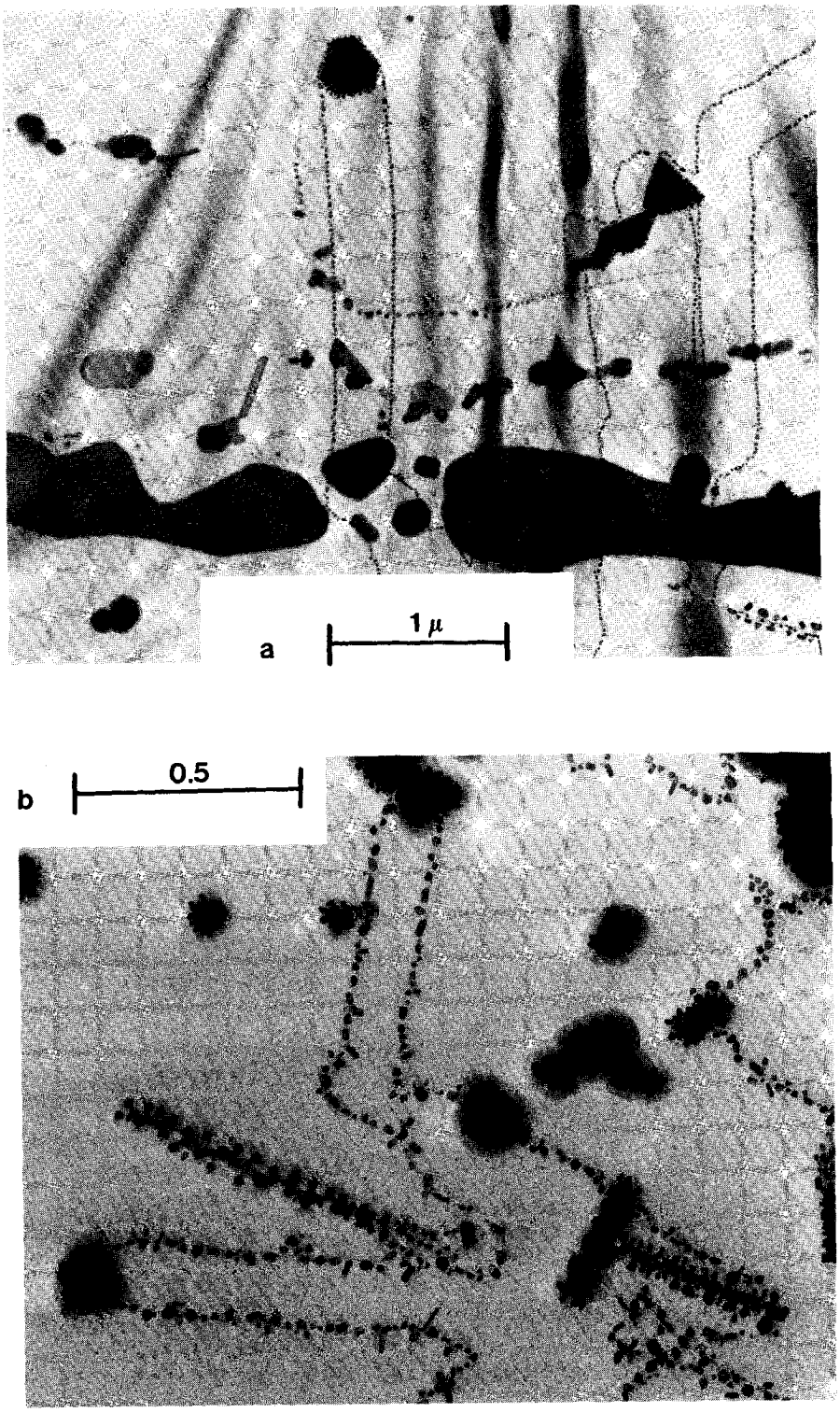

FIG. 6. Monolayer channels carved by vanadium oxide at 600°C in 0.1 atm O_2 for 16.5 min by large (a) and small (b) particles; (a) also shows patches of catalyst on the opposite side of the graphite sample (see more details in Fig. 3 caption).

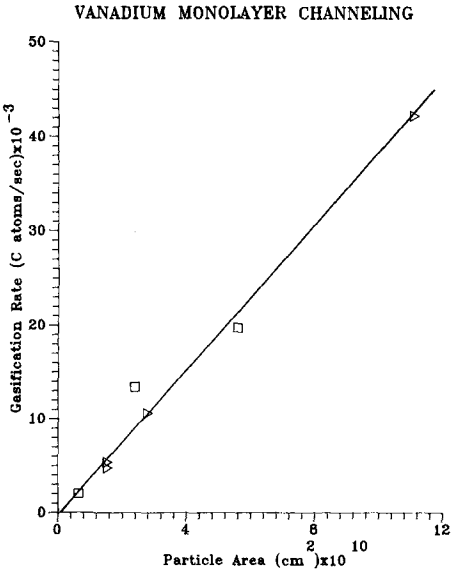

FIG. 7. Carbon gasification rate versus surface area of catalyst exposed to O_2 for reaction at 600°C in 0.1 atm O_2. Catalyst was deposited as V_2O_5 (triangles) and as V metal (squares).

limiting step. This step may be expressed as $V_6O_{13} + O_2 \rightarrow 3V_2O_5$.

Monolayer Edge Recession by V_2O_5

Another catalytic action by V_2O_5 (or V) in the catalyzed graphite–O_2 reaction is catalyzed monolayer etch pit growth. Monolayer etch pits in the uncatalyzed graphite–O_2 reaction are round and are formed at an edge recession rate of 0.026 nm/s at 600°C and 0.1 atm O_2 (*18, 28*). The vanadium catalyzed monolayer etch pits take a unique elongated hexagonal shape and have an edge recession rate up to 110 times higher than that of the uncatalyzed reaction.

Figure 8 shows a typical vanadium catalyzed monolayer etch pit. The monolayer etch pits are initiated from lattice vacancies on the surface graphite layer (*4, 18*). An additional inner pit will be produced after a vacancy in the second layer is exposed (*4,*

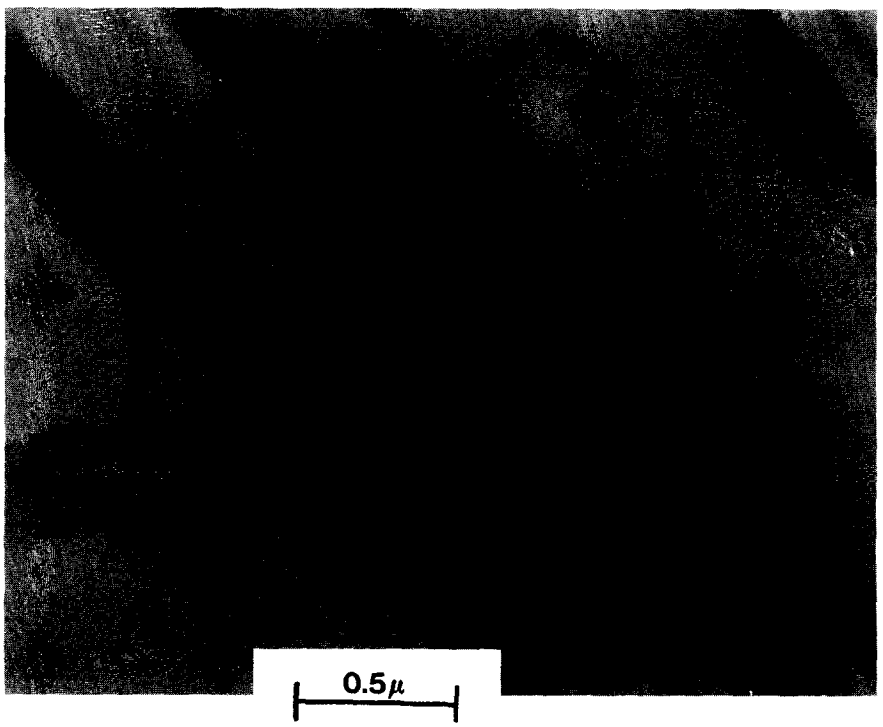

FIG. 8. Monolayer etch pit formed by V_2O_5 catalyst on graphite at 600°C in 0.1 atm O_2 for 16.5 min (see more details in Fig. 3 caption).

18). The elongated hexagonal pit on the second graphite layer (shown as the inner pit) was always inverted in orientation relative to the outer pit, illustrated typically by Fig. 9. Selected-area electron diffraction in the TEM showed that all etch pits were composed of $\langle 11\bar{2}0 \rangle$ (zig-zag) edges. The elongated hexagonal pit exhibits two different reaction rates with the shorter-length face of the hexagon having a higher edge recession rate than the longer-length face. The pits measured displayed a large variation in rates from short face = 0.32 nm/s and long face = 0.20 nm/s, to short face = 2.8 nm/s and long face = 1.9 nm/s. However, the ratio of (short-face rate) to (long-face rate) remained constant at a value of 1.5 ± 0.1. The variation in this ratio was due to experimental scatter of the data and showed no correlation to overall edge recession rate.

The intriguing question that arises is why is there such a substantial difference in reactivity between zig-zag faces on a monolayer step of graphite? To understand the difference in reactivity the stacking structure of the graphite basal planes must be understood. Figure 10 is a schematic representation of the relative positions of two basal planes, showing the ABAB . . . stacking of the basal planes of β-graphite. In Fig. 10, the top (surface) layer is represented by solid lines and solid circles, and the dashed lines and open circles represent the second layer. The thick solid line represents the edge of two adjacent faces which bound the hexagonal etch pit. Line AB connects the surface atoms of one side whereas line BC connects those of the adjacent side; these surface atoms are active sites as they possess a free sp^2 electron and are bonded to only two other carbon atoms. Figure 10 shows that these two adjacent edges are in fact different with respect to the position of carbon atoms in the basal plane directly below. The active edge atoms on line AB have a carbon atom directly below whereas those on line BC do

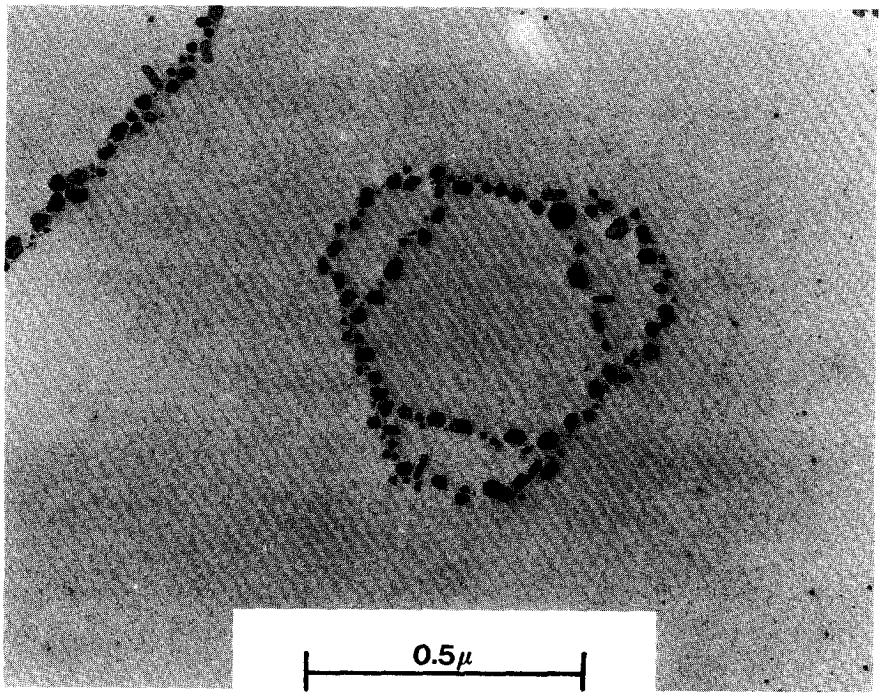

FIG. 9. Same as Fig. 8 except time = 14 min. The inner pit is initiated from a vacancy in the second graphite layer and its shape is inverted relative to the outer pit.

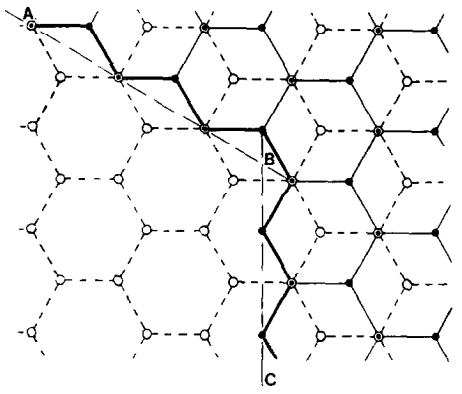

FIG. 10. Schematic representation of two graphite layers: the top layer by solid circles and solid lines, and the layer beneath by dashed lines and circles. AB and BC represent two adjacent edges of a hexagonal etch pit, showing they are in fact different.

not. This also explains the inverted shape for the inner pit, shown in Fig. 9.

Two important questions need to be addressed: (1) How do the atoms (3.35 Å) below affect the reactivity of the edge atoms? (2) Why is there such a large variation in the overall edge recession rate between edge AB and edge BC?

For uncatalyzed gas–carbon reactions, regularly shaped hexagonal monolayer etch pits are produced by water vapor (*18*) and by atomic oxygen (*30*), bound by zig-zag edges. Thus, these uncatalyzed reactions do not exhibit differences in the reactivities of the two different zig-zag edges represented by lines AB and BC. This fact indicates that the difference in reactivity was caused by the interactions of these edges with the vanadium oxide catalyst.

Qualitative observations of the gold-decorated graphite suggest that pits are formed by a small amount of vanadium oxide wetting the monolayer steps. A TEM picture of the reacted graphite with finely decorated gold nuclei is shown in Fig. 11. Double lines of gold nuclei are decorated on

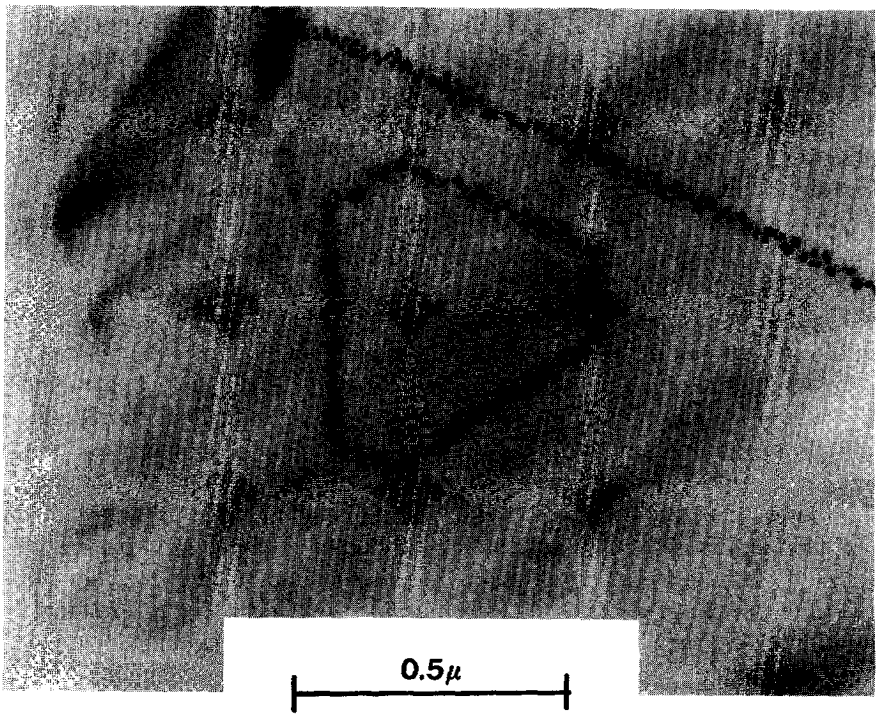

FIG. 11. Fine gold nuclei decorated on a monolayer etch pit and a step in vanadium oxide catalyzed oxidation at 600°C, 0.1 atm O_2 and 15 min. A thin film of vanadium oxide is decorated on the steps and the two edges of the film are decorated by gold nuclei.

each monolayer step. This indicates that a thin film (forming a strip) of vanadium oxide was decorated on each monolayer step and the two edges of the vanadium oxide film were decorated by gold nuclei. The smaller etch pits did not clearly exhibit the double-line gold nuclei, indicating that there were smaller amounts of catalyst wetting on the steps. This suggests that the rate of monolayer edge recession is directly proportional to the amount of catalyst wetting on the edge, which is also the reason for the large variation of the sizes of the catalyzed monolayer pits. The above discussion is consistent with the observation on the vanadium catalyzed deep-layer edge recession (*22*), in which a vanadium oxide film wetted the deep edge. Following this discussion, it appears that the two different monolayer edges (represented by lines AB and BC in Fig. 10) received different amounts of vanadium oxide decoration, probably caused by different interaction energies between the wetting catalyst and the two different edges. The more rapidly receding step has a higher interaction energy with vanadium oxide and hence receives a larger amount of catalyst. The redox mechanism discussed in the preceding section should also be operative in edge recession.

Relative Contribution to Total Rates

The catalyst deep channeling action has been studied in various gases extensively and is well understood (*7*). The monolayer channeling action by group VIII metals in the carbon–hydrogen reaction was studied in this laboratory (*15–17*) and it was concluded that the relative contribution by the monolayer channeling action to the total reaction rate was at least as important as that by deep channeling action (*17*). The same comparison will be made here for the graphite–oxygen reaction between the two channeling actions.

In this study, the temperatures for the three catalysts (Pt, Cu, and V_2O_5) were chosen to be the same as those at which the deep channeling action was studied by Baker *et al.* While a low oxygen pressure (of 5 Torr) was required in Baker's TEM environmental reactor, a convenient partial pressure of 0.1 atm was used in our monolayer channeling study. However, as in the graphite–hydrogen reaction (*15–17*), results for the Pt-catalyzed reaction indicate that oxygen partial pressure does not influence the monolayer channeling speeds. This can be expected from the knowledge on the rate-limiting steps for monolayer channeling as discussed in the foregoing. The monolayer channeling speed for Pt particles at 0.02 atm O_2 and 750°C was 23 nm/s (*31*), compared to 24 ± 2 nm/s at 0.1 atm and 750°C.

In comparing the relative contribution of the two channeling actions, two factors must be considered: the rate of carbon gasification per channeling particle, and the relative numbers of particles undergoing the two actions.

For deep channeling by Pt particles at 750°C, Baker *et al.* (*20*) only gave the rate for a particle size of 20 nm as 3 nm/s. The channel depth was not given, but may be reasonably assumed as $\frac{1}{2}$ of the particle size. Thus, the rate for deep channeling by this particle was 6.9×10^4 carbon atoms/s. For the same sized particle undergoing monolayer channeling at the same temperature, a linear speed of 24 nm/s results in 1.8×10^4 carbon atoms/s. The deep channeling speed is, however, inversely proportional to particle size for all catalysts studied (e.g., Pd in Ref. (*20*), but the size dependence for Pt was not studied (*20*)). On the contrary, the monolayer channeling speed for Pt is independent of size. Consequently, for larger particle sizes, monolayer channeling would contribute more than deep channeling to the overall reaction by particles of the same size.

A similar comparison may be made for Cu. The rate given by Baker *et al.* (*21*) was 1.6 nm/s for a 25-nm particle at 550°C, or 4.6×10^4 carbon atoms/s. The monolayer channeling rate was 45 nm/s, or 4.3×10^4

carbon atoms/s. Again, for particles larger than 25 nm, monolayer channeling would contribute more to the overall reaction than deep channeling.

For channeling by V_2O_5 (or V_6O_{13}), our results have shown that surface oxidation of the catalyst particle is the rate-limiting step, hence the rate of gasification per catalyst surface area is a constant. No deep channeling rates for V_2O_5 were given by Baker *et al.* (*22*), but the mechanism for deep channeling is expected to be like that for monolayer channeling. Thus, the amounts of carbon gasified per second per particle should be the same by the same sized particles undergoing two different channeling actions.

As discussed previously, for a reaction taking place in a mixture of graphite and catalyst powders, the number of catalyst particles undergoing monolayer channeling is far greater than that for deep channeling (*17*). Therefore, it is a reasonable conclusion that the relative contribution by monolayer channeling to the overall oxidation rate is at least as important as that by deep channeling. This comparison is made for O_2 partial pressure at 5 Torr.

DISCUSSION

Catalyst particles cut monolayer channels to gasify carbon on the basal plane of graphite in the graphite–oxygen reaction. The monolayer channeling action could not be detected in previous studies of deep-layer channeling using controlled-atmosphere TEM, and can be rendered visible by gold decoration.

The rate-limiting steps for monolayer channeling in graphite oxidation are different from and more complex than that of deep channeling. The rate-limiting step for monolayer channeling by Pt is the breakage of carbon–carbon bonds at the wetting interface between edge carbon and Pt. An oxygen transfer or redox mechanism is operative for monolayer channeling by vanadium oxide. The edge carbon adjacent to vanadia is oxidized by vanadia to gaseous products, and oxygen is replenished from the gas phase to the surface of the particle, which is subsequently transported to the reduced vanadia adjacent to edge carbon. The bulk of the vanadium oxide particle remains in the reduced state of V_6O_{13}. Oxidation of the catalyst surface is the rate-limiting step for channeling. A similar redox mechanism may or may not be operative in monolayer channeling by CuO. However, the rate-limiting step is either the reaction at the interface of CuO and edge carbon or the breakage of the carbon–carbon bond at the same interface. In addition to the monolayer channeling action, vanadium oxide also produces monolayer etch pits with a unique elongated hexagonal shape, which are bound by $\langle 11\bar{2}0 \rangle$ (zig-zag) graphite edges. This action is referred to as catalyzed monolayer edge recession, caused by various amounts of vanadium oxide wetting on the edges. By considering the stacking structure of graphite, it is shown that two adjacent zig-zag edges (forming a 120° angle) bounding the pits are in fact different, which results in different recession rates (at a ratio of 1.5) and hence the elongated hexagon shape.

ACKNOWLEDGMENT

The authors are indebted to the National Science Foundation for Support (Grant CBT-8703677).

REFERENCES

1. Walker, P. L., Jr., Rusinko, F., Jr., and Austin, L. G., *in* "Advances in Catalysis," Vol. 11, p. 133. Academic Press, New York, 1959.
2. Walker, P. L., Jr., Shelef, M., and Anderson, R. A., *in* "Chemistry and Physics of Carbon" (P. L. Walker, Ed.). Dekker, New York, 1968.
3. Hennig, G. R., *in* "Proceedings, Conf. Carbon, 1st and 2nd, Buffalo, 1953, 1955," p. 112 (1956).
4. Hening, G. R., *in* "Chemistry and Physics of Carbon" (P. L. Walker, Jr., Ed.), Vol. 2. Dekker, New York, 1966.
5. Baker, R. T. K., *Catal. Rev. Sci. Eng.* **19**(2), 161 (1979).
6. Thomas, J. M., *in* "Chemistry and Physics of Carbon" (P. L. Walker, Jr., Ed.), Vol. 1. Dekker, New York, 1965.

7. Baker, R. T. K., *in* "Carbon and Coal Gasification—Science and Technology" (J. L. Figuereido and J. A. Moulijn, Eds.), Martinus Nijhoff, NATO ASI Series E, No. 105, p. 231 (1986).
8. Hennig, G. R., *J. Inorg. Nucl. Chem.* **24,** 1129 (1962).
9. McKee, D. W., *in* "Chemistry and Physics of Carbon" (P. L. Walker, Jr., and P. A. Thrower, Eds.), Vol. 16. Dekker, New York, 1980.
10. Keep, C. W., Terry, S., and Wells, M., *J. Catal.* **66,** 451 (1980).
11. Coates, D. J., Evans, J. W., Cabrera, A. L., Somorjai, G. A., and Heinemann, H., *J. Catal.* **80,** 215 (1983).
12. Harris, P. S., Feates, F. S., and Reuben, B. G., *Carbon* **11,** 565 (1973).
13. Baker, R. T. K., *Carbon* **24,** 715 (1986).
14. Yang, R. T., and Wong, C., *J. Catal.* **85,** 154 (1984).
15. Goethel, P. J., and Yang, R. T., *J. Catal.* **101,** 342 (1986).
16. Goethel, P. J., and Yang, R. T., *J. Catal.* **108,** 356 (1987).
17. Goethel, P. J., and Yang, R. T., *J. Catal.* **111,** 220 (1988).
18. Yang, R. T., *in* "Chemistry and Physics of Carbon" (P. A. Thrower, Ed.), Vol. 19. Dekker, New York, 1984.
19. Goethel, P. J., Ph.D. dissertation, State University of New York at Buffalo, Buffalo, NY, 1988.
20. Baker, R. T. K., France, J. A., Rouse, L., and Waite, R. J., *J. Catal.* **41,** 22 (1976).
21. Baker, R. T. K., and Chludzinski, J. J., *Carbon* **19,** 75 (1981).
22. Baker, R. T. K., Thomas, R. B., and Wells, M., *Carbon* **13,** 141 (1975).
23. Holstein, W. L., and Boudart, M., *Fuel* **62,** 162 (1983).
24. McKee, D. W., *Carbon* **8,** 623 (1970).
25. Goethel, P. J., Tsamopoulos, J. A., and Yang, R. T., *AIChE J.* **35,** 686 (1989).
26. Holstein, W. L., and Boudart, M., *J. Catal.* **72,** 328 (1981).
27. Holstein, W. L., and Boudart, M., *J. Catal.* **75,** 337 (1982).
28. Yang, R. T., and Wong, C., *J. Chem. Phys.* **75,** 4471 (1981).
29. McKee, D. W., *Carbon* **8,** 131 (1970).
30. Wong, C., Yang, R. T., and Halpern, B. L., *J. Chem. Phys.* **78,** 3325 (1983).
31. Pan, Z. J., Goethel, P. J., and Yang, R. T., unpublished results, SUNY at Buffalo, 1989.